# Uncovering Droop Control Laws Embedded Within the Nonlinear Dynamics of Van der Pol Oscillators

Mohit Sinha, *Student Member, IEEE*, Florian Dörfler, *Member, IEEE*,
Brian B. Johnson, *Member, IEEE*, and Sairaj V. Dhople, *Member, IEEE*

***Abstract*—This paper examines the dynamics of power-electronic inverters in islanded microgrids that are controlled to emulate the dynamics of Van der Pol oscillators. The general strategy of controlling inverters to emulate the behavior of nonlinear oscillators presents a compelling time-domain alternative to ubiquitous droop control methods which presume the existence of a quasistationary sinusoidal steady state and operate on phasor quantities. We present two main results in this paper. First, by leveraging the method of periodic averaging, we demonstrate that droop laws are intrinsically embedded within a slower time scale in the nonlinear dynamics of Van der Pol oscillators. Second, we establish the global convergence of amplitude and phase dynamics in a resistive network interconnecting inverters controlled as Van der Pol oscillators. Furthermore, under a set of nonrestrictive decoupling approximations, we derive sufficient conditions for local exponential stability of desirable equilibria of the linearized amplitude and phase dynamics.**

***Index Terms*—Averaging, droop control, nonlinear oscillator circuits, synchronization, Van der Pol oscillators.**

## I. Introduction

An islanded inverter-based microgrid is a collection of heterogeneous dc energy resources, for example, photovoltaic (PV) arrays, fuel cells, and energy-storage devices, interfaced to an ac electric distribution network and operating independently from the bulk power system. Energy conversion is typically managed by semiconductor-based power-electronic voltage-source inverters. The goal of decentralized real-time control is to regulate the inverters' terminal voltage amplitude and frequency to realize a stable power system while achieving a fair and economic sharing of the network load.

Manuscript received November 21, 2014; revised August 2, 2015; accepted October 19, 2015. Date of publication November 24, 2015; date of current version June 16, 2017. This work was supported in part by the National Science Foundation under the CAREER award ECCS-CAR-1453921 and Grant ECCS-1509277, in part by the Office of Naval Research under Grant N000141410639, in part by ETH Zürich funds and the SNF Assistant Professor Energy Grant #160573, and in part by the Laboratory Directed Research and Development Program at NREL and the U.S. Department of Energy under Contract No. DE-AC36-08-GO28308 with NREL.

M. Sinha and S. V. Dhople are with the Department of Electrical and Computer Engineering ,University of Minnesota, Minneapolis, MN 55455 USA (e-mail: sinha052@UMN.EDU; sdhople@UMN.EDU).

F. Dörfler is with the Automatic Control Laboratory, ETH Zürich, 8092 Zürich, Switzerland (e-mail: dorfler@ETHZ.CH).

B. B. Johnson is with the Power Systems Engineering Center, National Renewable Energy Laboratory (NREL), Golden, CO 80401 USA (e-mail: brian.johnson@NREL.GOV).

Color versions of one or more of the figures in this paper are available online at http://ieeexplore.ieee.org.

Digital Object Identifier 10.1109/TCNS.2015.2503558

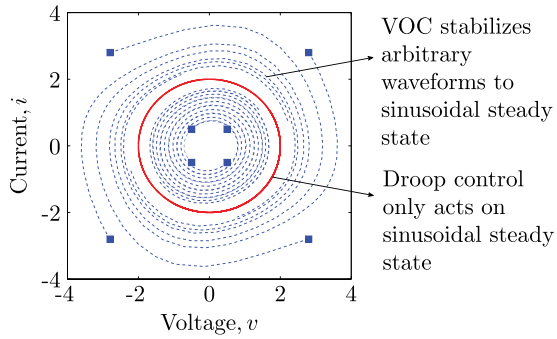


Fig. 1. VOC stabilizes arbitrary initial conditions to a sinusoidal steady state, while droop control acts on phasor quantities; only well defined in the sinusoidal steady state. One contribution of this work is to determine a set of parametric correspondences such that both approaches admit identical dynamics in sinusoidal steady state.

The vast majority of academic and industrial efforts approaches the real-time control challenge by means of *droop control* [1]–[4]. Drawing from the control of synchronous generators in bulk power systems, droop control linearly trades off the active and reactive power injection with the inverters' terminal voltage amplitude and frequency. In this paper, we focus on a communication-free decentralized control strategy wherein islanded inverters are regulated to mimic the dynamics of nonlinear limit-cycle oscillators [5]–[8]. This method is inspired by synchronization phenomena in complex networks of coupled oscillators, and is called *virtual oscillator control* (VOC). In general, VOC is executed by programming nonlinear differential equations of limit-cycle oscillators onto inverters' microcontrollers, and utilizing pertinent sinusoidally varying oscillator dynamic states to construct the pulse-width modulation (PWM) control signal. It is worth emphasizing that VOC constitutes a *time-domain* approach and stabilizes arbitrary initial conditions to a sinusoidal steady state. As such, it is markedly different from droop control which operates on phasor quantities and presumes the existence of a quasistationary ac steady state (for computing average active-and reactive power); see Fig. 1. Both generation and load can be expected to vary rapidly in low-inertia microgrids and, therefore, notions of average active/reactive power and even electrical frequency may not be well defined. To address the application-oriented challenges of regulating voltages and frequencies under rapidly varying conditions, and the analysis-oriented challenges of contending with electrical system definitions that are only valid in a well-behaved sinusoidal steady state, we offer VOC as a compelling alternative to droop control. See also [9] and [10] for similar time-domain control strategies.

Extending our previous efforts in [5]–[8] where we focused on deadzone oscillators, in this paper, we investigate the voltage dynamics of power-electronic inverters controlled to emulate the dynamics of Van der Pol oscillators (essentially, smooth cubic polynomial realizations of deadzone oscillators). Unless stated otherwise, in subsequent discussions where we reference VOC, we imply that the control strategy is implemented with Van der Pol oscillators. Also, inverters controlled with this approach are called virtual-oscillator controlled (VO-controlled) inverters. Since Van der Pol oscillators offer a stable limit cycle that can be engineered to be close to sinusoidal, inverters can rapidly stabilize arbitrary initial conditions to the sinusoidal steady state. Furthermore, coupled Van der Pol oscillators tend to synchronize without any external forcing or extraneous communication [11], [12] and, hence, emulating their dynamics presents an effective strategy to realize a stable ac microgrid.

We provide two main contributions in this paper: First, a correspondence is established between VOC and droop control by obtaining conditions under which the respective voltage dynamics at the inverter terminals—close to the sinusoidal steady state—are identical. To bridge the temporal gap between droop control and VOC, we average the periodic nonlinear oscillator dynamics to focus on ac-cycle time scales [13]. In addition to yielding insightful circuit-theoretic interpretations for droop control, our analysis highlights the choice of design parameters that ensure VO-controlled inverters mimic the behavior of droop-controlled inverters close to the quasistationary sinusoidal steady state and vice-versa (see Fig. 1). This allows us to leverage insights on the optimal choice of droop coefficients [14] to design VO-controlled inverters that achieve load sharing or economic optimality in steady state.

The second contribution of this paper is to demonstrate the convergence of the averaged terminal voltage amplitude and phase dynamics of VO-controlled inverters in resistive networks using a gradient-sytem formulation in concert with LaSalle's invariance principle. Our focus on resistive interconnection lines is motivated by the fact that we envision these controllers to be of interest in distribution networks (where transmission-line $r/x$ ratios are relatively high). As a recent extension, we have examined how suitably formulated coordinate transformations can be leveraged to extend the approach to other networks [15]. Under a set of nonrestrictive decoupling assumptions on the phase and amplitude dynamics—valid in unstressed networks with a nearly uniform voltage profile and approximately equal phase angles [1], [2], [16]–[19]—we also present sufficient conditions for local exponential stability of potentially desirable equilibria of the linearized and averaged VO-controlled inverter dynamics.

Within the realm of analytical approaches that investigate stability and synchronization in this application domain, for the deadzone-type oscillators and parallel-connected inverters considered in [5]–[8], we utilized small-gain-type arguments to prove synchronization. These results were generalized in terms of oscillator type and network topology recently in [20] by leveraging structural and spectral properties of a network reduction procedure called Kron reduction [21]. Related work in [9] and [10] employed similar arguments based on incremental passivity. From a dynamical systems perspective, we establish a connection between limit-cycle oscillators (VO-controlled inverters) and phase oscillators (droop-controlled inverters) by means of coordinate transformations and averaging. For Van der Pol oscillators, similar connections and synchronization analyses date back to [11] and have recently been surveyed in the tutorial [22]. In addition, averaging methods have recently been applied to study synchronization in Liénard-type oscillators [23], which include Van der Pol oscillators as a particular case. It is also worth mentioning that similar averaging methods have been applied to extract small-signal state-space models for dc–dc power-electronic converters [24]–[28]. Finally, we emphasize that the averaging analysis adopted here applies to general planar Liénard-type limit-cycle oscillators which include Van der Pol oscillators as a particular case [29].

Related to this work, for droop-controlled inverters in radial lossless microgrids under the assumption of constant voltage amplitudes, analytic conditions for proportional power sharing and synchronization have recently been derived by applying results from the theory of coupled oscillators in [14] and [30]. Conditions for voltage stability for a lossless parallel microgrid with one common load have been derived in [31]. A decentralized linear matrix inequality-based control design for guaranteeing network stability considering variable voltage amplitudes and phase angles for meshed networks while accounting for power sharing has been described in [32].

The remainder of this manuscript is organized as follows. Section II establishes notation and relevant mathematical preliminaries. In Section III, we introduce droop control and VOC, and derive parametric conditions under which inverter dynamics controlled with the two approaches are identical. Next, in Section IV, we establish global convergence of solutions for VO-controlled inverters in resistive networks; we also derive conditions for the exponential stability of linearized and decoupled amplitude and phase dynamics. Finally, we provide numerical simulations in Section V, and conclude this paper in Section VI by highlighting directions for future work.

## II. Notation and Preliminaries

In this section, we introduce the electrical system fundamentals that we will find useful in subsequent developments. Particularly, we model the inverter voltage in a rotating frame of reference specified by the nominal system frequency (a global variable). It is in this reference frame that we examine the voltage phasors to compute the instantaneous active and reactive power. Using these real-time signals, we will subsequently leverage periodic averaging to extract average active and reactive power. This will aid us in conclusively drawing links between averaged VOC dynamics and droop control.

### A. Electrical System Fundamentals

The nominal system frequency is denoted by $\omega$, and for the $j$th inverter, the instantaneous phase angle $\phi_j$ evolves as

$$\frac{d\phi_j}{dt} = \omega + \frac{d\theta_j}{dt} \tag{1}$$

where $\theta_j$ represents the phase offset with respect to the rotating reference frame established by $\omega$. Denote the instantaneous

current injected by the $j$th inverter by $i_j(t)$ and its instantaneous terminal voltage by $v_j(t)$. Since we are primarily interested in harmonic signals, we parameterize the instantaneous voltage as $v_j(t) := r_j(t)\cos(\omega t + \theta_j(t))$, where $r_j(t)$ is the instantaneous terminal voltage amplitude. We define the instantaneous active and reactive power injections [33], [34]

$$\begin{aligned} P_j(t) &:= v_j(t) i_j(t) = r_j(t)\cos\left(\omega t + \theta_j(t)\right) i_j(t) \\ Q_j(t) &:= v_j\left(t - \frac{\pi}{2}\right) i_j(t) = r_j(t)\sin\left(\omega t + \theta_j(t)\right) i_j(t). \end{aligned} \quad (2)$$

Assuming the fundamental frequency of the current injected by the $j$th inverter is $\omega$, the average active and reactive power over an ac cycle (of period $2\pi/\omega$) are then given by

$$\overline{P}_j = \frac{\omega}{2\pi}\int_{s=0}^{\frac{2\pi}{\omega}} P_j(s)ds,\ \overline{Q}_j = \frac{\omega}{2\pi}\int_{s=0}^{\frac{2\pi}{\omega}} Q_j(s)ds. \quad (3)$$

In general, the time average of a periodic signal $u_j$ with period $T$ is denoted by $\overline{u}_j$, and defined as

$$\overline{u}_j := \frac{1}{T}\int_0^T u_j(t)dt. \quad (4)$$

Subsequent developments will leverage signals represented in the scaled time coordinates $\tau = \omega t$, and for the continuous time signal $x$, we will denote $\dot{x} = (d/d\tau)x$.

### B. Mathematical Notation

For the $N$-tuple $\{x_1, \ldots, x_N\}$, denote $x = [x_1, \ldots, x_N]^{\mathrm{T}}$ to be the corresponding column vector; $(\cdot)^{\mathrm{T}}$ denotes transposition. The cardinality of the set $\mathcal{X}$ is denoted by $|\mathcal{X}|$; $[X]_{ij}$ isolates the entry in the $i$th row and $j$th column of matrix $X$. $\mathbb{R}^N$ is the space of $N \times 1$ real-valued vectors, $\mathbb{T}^N$ is the $N$-torus. Given a scalar function $f(x)$, $\nabla_x f(x)$ returns the gradient $[(\partial f/\partial x_1), \ldots, (\partial f/\partial x_n)]^{\mathrm{T}}$. Finally, $\mathrm{diag}\{x_1, \ldots, x_N\}$ denotes a diagonal matrix with diagonal entries given by $x_1, \ldots, x_N$.

## III. Correspondence Between Droop Control and VOC for Inverter Control

In this section, we derive the design parameters that can ensure VO-controlled inverters emulate the behavior of droop-controlled inverters close to the quasistationary sinusoidal steady state and vice-versa. The results presented in this section demonstrate the backward compatibility of VOC with droop. Consequently, a wealth of literature in droop control (for instance, the choice of optimal droop coefficients to ensure load sharing or economic optimality) could, in fact, be leveraged to inform design strategies for VOC. We begin with a brief overview of VOC and droop control.

### A. VOC Implemented with a Van der Pol Oscillator

Consider the Van der Pol oscillator to constitute the virtual oscillator circuit for inverter control as shown in Fig. 2. Note that Fig. 2 is meant to highlight a circuit interpretation of the oscillator dynamics; the controller is actually implemented by programming the corresponding oscillator dynamics (we comment on these shortly) onto the inverter's microcontroller and by using relevant states to construct the PWM signal.

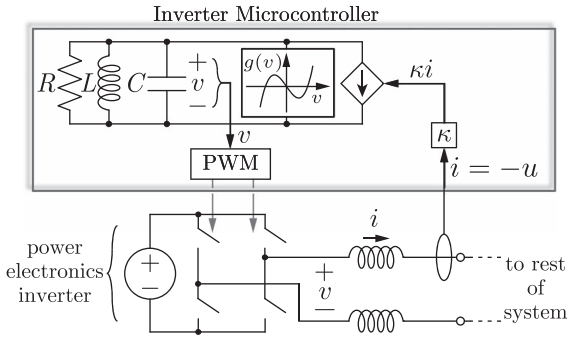


Fig. 2. Implementation of VOC for a single-phase power-electronic inverter. The Van der Pol oscillator is composed of a parallel RLC circuit, and a nonlinear voltage-dependent current source $g(v)$. The capacitor voltage is utilized as the PWM modulation signal.

The Van der Pol oscillator is composed of a parallel RLC circuit and a nonlinear voltage-dependent current source $g(v) := \sigma v - kv^3$, where $v$ denotes the inverter-terminal voltage and $\sigma, k$ are positive constants. Leveraging Kirchoff's circuit equations, we write the dynamics of the oscillator as[1]

$$\begin{aligned} L\frac{di_L}{dt} &= v \\ C\frac{dv}{dt} &= \sigma v - kv^3 - \frac{v}{R} - i_L + \kappa u(t) \end{aligned} \quad (5)$$

where $u(t)$ is the current input to the Van der Pol oscillator (see Fig. 2), and $\kappa$ is the *current gain*. In particular, the inverter output current is scaled by $\kappa$, and this is extracted from the Van der Pol oscillator that forms the inverter controller. In the scaled time coordinates $\tau = t/\sqrt{LC}$, the dynamics of the oscillator are therefore captured by the following equation:

$$\ddot{v} - \sqrt{\frac{L}{C}}\left(\sigma - \frac{1}{R}\right)\left(1 - \frac{3k}{\left(\sigma - \frac{1}{R}\right)}v^2\right)\dot{v} + v = \kappa\sqrt{\frac{L}{C}}\dot{u}(\tau). \quad (6)$$

For the purpose of analysis, we compactly describe the system in (6) as

$$\ddot{v} - \varepsilon\alpha(1 - \beta v^2)\dot{v} + v = \kappa\varepsilon\dot{u}(\tau) \quad (7)$$

by defining the following parameters:

$$\varepsilon := \sqrt{\frac{L}{C}}, \quad \alpha := \sigma - \frac{1}{R}, \quad \beta := \frac{3k}{\left(\sigma - \frac{1}{R}\right)}. \quad (8)$$

With this notation in place, Liénard's condition [12] for ensuring a stable limit cycle in the system (7) requires positive damping at the origin, that is, $\alpha = \sigma - 1/R > 0$. In the so-called quasiharmonic limit, that is, $\varepsilon \searrow 0$, the model (7) reduces to a forced harmonic oscillator with unit frequency. In the original time scale $t = \tau\sqrt{LC}$, this natural frequency of oscillation is $1/\sqrt{LC}$. By standard regular perturbation arguments [13, Theor. 10.1], this correspondence can also be

[1]For notational simplicity, we drop the subscript from electrical quantities and parameters that indexes the inverter in this section.

made for $\varepsilon$ sufficiently small. In subsequent developments, with reference to (1), and to compare the droop-control system (13) and the VOC system (6), we set $\omega = 1/\sqrt{LC}$.

We begin by establishing a state-space model in Cartesian coordinates; choosing a scaled version of the inductor current and capacitor voltage as states $x := \varepsilon i_L$ and $y := v$, we get

$$\dot{x} = y,\ \dot{y} = -x + \varepsilon\alpha h(y) + \varepsilon\kappa u(\tau) \tag{9}$$

where we define $h(y) := y - \beta(y^3/3)$. Next, we transform the model (9) to polar coordinates by defining $x = r\sin(\phi)$ and $y = r\cos(\phi)$. We recover the following dynamics in polar coordinates:[2]

$$\begin{aligned}\dot{r} &= \varepsilon\left(\alpha h\left(r\cos(\phi)\right) + \kappa u(\tau)\right)\cos(\phi)\\ \dot{\phi} &= 1 - \varepsilon\left(\frac{\alpha}{r}h\left(r\cos(\phi)\right) + \frac{\kappa u(\tau)}{r}\right)\sin(\phi).\end{aligned} \tag{10}$$

In ensuing discussions, we will leverage (10) written in the original time coordinates, with the nominal frequency of oscillation $\omega = 1/\sqrt{LC}$ and phase offset as defined in (1)

$$\begin{aligned}\frac{dr}{dt} &= \frac{1}{C}\left(\alpha h\left(r\cos(\omega t+\theta)\right) + \kappa u(t)\right)\cos(\omega t+\theta)\\ \frac{d\theta}{dt} &= \omega - \left(\frac{\alpha}{rC}h\left(r\cos(\omega t+\theta)\right) + \frac{\kappa u(t)}{rC}\right)\sin(\omega t+\theta).\end{aligned} \tag{11}$$

*Remark 1 (Controller Implementation):* Essentially, (11) and (13) describe the controller dynamics of the per-phase equivalent circuit at the inverter terminals; the signal $v = y = r\cos(\phi)$ can be utilized for control of single-phase inverters [8] (Fig. 2). For three-phase settings, a balanced set of PWM modulation signals $m_{\rm a}, m_{\rm b}, m_{\rm c}$ is obtained as follows:

$$\begin{bmatrix} m_{\rm a}\\ m_{\rm b}\\ m_{\rm c}\end{bmatrix} = \Sigma^{\rm T}\begin{bmatrix} r\cos(\phi)\\ r\sin(\phi)\end{bmatrix},\quad \Sigma := \begin{bmatrix} 1 & -\frac{1}{2} & -\frac{1}{2}\\ 0 & \frac{\sqrt{3}}{2} & -\frac{\sqrt{3}}{2}\end{bmatrix}. \tag{12}$$

The matrix $\Sigma$ implements a coordinate transformation from polar to abc coordinates [6], [35]. ■

### B. Droop Control

For resistive networks, droop control linearly trades off frequency deviation versus reactive power; and inverter terminal voltage amplitude versus active power [2], [36]

$$\frac{d}{dt}\overline{\theta}_j = n_j\left(\overline{Q}_j - \overline{Q}_j^*\right),\ \overline{r}_j - \overline{r}_j^* = m_j\left(\overline{P}_j^* - \overline{P}_j\right) \tag{13}$$

where $\overline{Q}_j^*$ and $\overline{P}_j^*$ are the per-phase average reactive power and active power setpoints, respectively; $\overline{r}_j^*$ is the terminal voltage-amplitude setpoint; and $n_j, m_j \in \mathbb{R}_{>0}$ are reactive power and active power droop coefficients, respectively. As expressed in (13), we assume that the droop laws are executed with ac-cycle averages of active and reactive power. To preserve the generality of the ensuing discussions, we disregard the dynamics of additional low-pass filters, voltage controllers, and current controllers in experimental implementations [3]; however, these could be included in the analysis readily.

[2]This bijective change of coordinates is well defined (and leads to smooth dynamics) whenever $r \neq 0$ or, equivalently, $[x, y]^{\rm T} \neq 0$. In Theorem 2, we establish well-posedness conditions that focus on convergence of the amplitude dynamics to an equilibrium that excludes the origin.

### C. Uncovering Droop Laws in Averaged VOC Dynamics

Consider two microgrids, each with $N$ identical inverters, identical network configurations, and loads. All inverters in one microgrid are controlled with VOC (11), and the inverters in the other are controlled with droop control (13). For the $j$th inverter, denote the difference in voltage amplitudes and phase offsets in the two inverter-control strategies by

$$e_r(t) = \bar{r}_j - r_j(t),\ e_\theta(t) = \bar{\theta}_j(t) - \theta_j(t) \tag{14}$$

where $\bar{r}_j$ and $\bar{\theta}_j(t)$ are the amplitudes and phases as used in droop control (13), and $r_j(t)$ and $\theta_j(t)$ are those in VOC (11).

In the following discussion, we analyze how the droop laws and coefficients should be designed so that the difference in the phase dynamics and steady-state equilibrium voltage profile of the two sets of inverters (controlled with VOC and droop) is of order $\mathcal{O}(\varepsilon) = \mathcal{O}(\sqrt{L/C})$. To bridge the time-scale separation between VOC (that is implemented in real time) and droop control (that presumes the existence of a quasi-stationary sinusoidal steady state), we average the VOC dynamics (11) (a detailed derivation is provided in Step 1 of the proof to Theorem 1 below) to arrive at the following description:

$$\frac{d}{dt}\overline{r}_j = \frac{\alpha}{2C}\left(\overline{r}_j - \frac{\beta}{4}\overline{r}_j^3\right) - \frac{\kappa_j}{C\overline{r}_j}\overline{P}_j \tag{15a}$$

$$\frac{d}{dt}\overline{\theta}_j = +\frac{\kappa_j}{C\overline{r}_j^2}\overline{Q}_j. \tag{15b}$$

The averaged VOC dynamics (15) enable us to compare the droop control laws in (13) with VOC (11).

We remark that due to the circuit interpretation of VOC adopted throughout the narrative, the dynamics of the voltage amplitude and frequency for the (virtual) oscillator are linked to active and reactive power that is sourced from the (physical) inverter. The subsequent analysis and results could very well have been presented by adopting a general state-space model for the controller, but persisting with the circuit-theoretic interpretation is essential to justify the physical relevance of our assumptions.

*Therem 1 (Correspondence Between Droop Control and VOC):* Consider two identical microgrids where all inverters in one microgrid are controlled with VOC (11), and the inverters in the other are droop controlled (13). Assume

A1) unique solutions to the droop-controlled system (13) and the averaged VOC system (15) exist in a time interval $t \in [0, t^*]$ of strictly positive length.

A2) the average active power delivered by the $j$th inverter in sinusoidal steady state $\overline{P}_{j,\rm eq}$ is bounded as

$$0 < \kappa_j\overline{P}_{j,\rm eq} < \frac{\alpha}{2\beta} \tag{16}$$

so that the average VOC dynamics (15) admit a non-negative amplitude equilibrium $\overline{r}_{j,\rm eq}$.

A3) the VO-controlled microgrid (11) and the droop-controlled microgrid (13) operate in steady state and the initial signal differences are of order $\varepsilon = \sqrt{L/C}$

$$e_r(0) \approx \mathcal{O}(\varepsilon) \quad \text{and} \quad e_\theta(0) \approx \mathcal{O}(\varepsilon).$$

Suppose the frequency-droop coefficient is picked as

$$n_j = \frac{\kappa_j}{\overline{r}_{j,\mathrm{eq}}^2 C} \tag{17}$$

and the average reactive power setpoint is set to zero $\overline{Q}_j^* = 0$. Suppose the voltage-droop coefficient is picked as

$$m_j = -\kappa_j \left( \alpha \left( \overline{r}_{j,\mathrm{eq}} - \frac{\beta}{2} \overline{r}_{j,\mathrm{eq}}^3 \right) \right)^{-1} \tag{18}$$

and the average active power and amplitude setpoints are picked as $\overline{P}_j^* = \overline{P}_{j,\mathrm{eq}}$ and $\overline{r}_j^* = \overline{r}_{j,\mathrm{eq}}$. Then, there exists an $\varepsilon^*$, such that for all $0 < \varepsilon < \varepsilon^*$, for all $t \in [0, t^*]$

$$e_r(t) \approx \mathcal{O}(\varepsilon) \text{ and } e_\theta(t) \approx \mathcal{O}(\varepsilon).$$

Assumption A1) is guaranteed for $\overline{r}_j(0) > 0$ due to local Lipschitz continuity, A2) can be met by design, and A3) is necessary for comparing the two strategies using averaging techniques.

The correspondences derived in Theorem 1 are asymptotic results based on a perturbation and averaging analysis for sufficiently small $\varepsilon = \sqrt{L/C}$. However, a small $\varepsilon$ also implies a weak (nonlinear) viscous damping in (7) and a slow convergence to the quasiharmonic limit cycle. In Section V-C, we show that the convergence rate is, in fact, inversely proportional to $\varepsilon$. Theorem 1 and the aforementioned discussion indicate that the droop laws (13) are recovered from the VOC dynamics (11) only on *slow* AC-cycle time scales, and when the dynamics of VO-controlled inverters are *deliberately decelerated*. Hence, on the limit cycle, the decelerated VOC subsumes droop control, but it is much faster in general. Finally, the correspondences established in (17) and (18) are formally valid only on a bounded time horizon $[0, t^*]$. The findings can be extended to an unbounded time horizon provided that the averaged system is exponentially stable [13]. In Section IV, we establish such exponential stability results.

*Proof:* The proof consists of three parts: 1) an averaging analysis of VOC; 2) a correspondence of the phase dynamics; and 3) a correspondence of the steady-state voltage amplitudes.

*1) Averaging the VOC Dynamics:* We begin by averaging the dynamics (7) of the VO-controlled microgrid. To this end, we first express (11) in the time coordinates $\tau = t/\sqrt{LC}$[3]

$$\begin{aligned} \dot{r} &= \varepsilon \left( \alpha h \left( r \cos(\tau + \theta) \right) + \kappa u(\tau) \right) \cos(\tau + \theta) \\ \dot{\theta} &= -\varepsilon \left( \frac{\alpha}{r} h \left( r \cos(\tau + \theta) \right) + \frac{\kappa u(\tau)}{r} \right) \sin(\tau + \theta). \end{aligned} \tag{19}$$

Note that the dynamical systems above are $2\pi$-periodic functions in $\tau$. In the quasiharmonic limit $\varepsilon \searrow 0$, we can apply standard averaging arguments using $\varepsilon$ as the *small parameter* to obtain the averaged dynamics [13]

$$\begin{aligned} \begin{bmatrix} \dot{\overline{r}} \\ \dot{\overline{\theta}} \end{bmatrix} &= \frac{\varepsilon}{2\pi} \int_0^{2\pi} \alpha h \left( \overline{r} \cos(\tau + \overline{\theta}) \right) \begin{bmatrix} \cos(\tau + \overline{\theta}) \\ -\frac{1}{\overline{r}} \sin(\tau + \overline{\theta}) \end{bmatrix} d\tau \\ &\quad + \frac{\varepsilon}{2\pi} \int_0^{2\pi} \kappa u(\tau) \begin{bmatrix} \cos(\tau + \overline{\theta}) \\ -\frac{1}{\overline{r}} \sin(\tau + \overline{\theta}) \end{bmatrix} d\tau = \varepsilon\alpha \begin{bmatrix} \frac{\overline{r}}{2} - \beta \frac{\overline{r}^3}{8} \\ 0 \end{bmatrix} \\ &\quad + \frac{\varepsilon}{2\pi} \int_0^{2\pi} \kappa u(\tau) \begin{bmatrix} \cos(\tau + \overline{\theta}) \\ -\frac{1}{\overline{r}} \sin(\tau + \overline{\theta}) \end{bmatrix} d\tau. \end{aligned} \tag{20}$$

The last line in (20) follows from:

$$\begin{aligned} &-\frac{\varepsilon}{2\pi\overline{r}} \int_0^{2\pi} \alpha h \left( \overline{r} \cos(\tau + \overline{\theta}) \right) \sin(\tau + \overline{\theta}) d\tau \\ &= \frac{\alpha\varepsilon}{2\pi} \left( \left[ \frac{1}{4} \cos(2\tau + 2\overline{\theta}) \right]_0^{2\pi} + \frac{\beta\overline{r}^2}{3} \left[ \cos^4(\tau + \overline{\theta}) \right]_0^{2\pi} \right) = 0. \end{aligned}$$

Transitioning (20) from $\tau$ to $t$ coordinates, we obtain

$$\begin{bmatrix} \frac{d\overline{r}}{dt} \\ \frac{d\overline{\theta}}{dt} \end{bmatrix} = \frac{\alpha}{C} \begin{bmatrix} \frac{\overline{r}}{2} - \beta \frac{\overline{r}^3}{8} \\ 0 \end{bmatrix} + \frac{\kappa\omega}{2\pi C} \int_0^{\frac{2\pi}{\omega}} u(t) \begin{bmatrix} \cos(\omega t + \overline{\theta}) \\ -\frac{1}{\overline{r}} \sin(\omega t + \overline{\theta}) \end{bmatrix} dt.$$

From Fig. 2, we recognize that the current sourced by the Van-der-Pol oscillator is $i(t) = -u(t)$, and we obtain

$$\begin{aligned} \begin{bmatrix} \frac{d\overline{r}}{dt} \\ \frac{d\overline{\theta}}{dt} \end{bmatrix} &= \frac{\alpha}{C} \begin{bmatrix} \frac{\overline{r}}{2} - \frac{\beta\overline{r}^3}{8} \\ 0 \end{bmatrix} + \frac{\kappa\omega}{2\pi C} \int_0^{\frac{2\pi}{\omega}} \begin{bmatrix} -i(t) \cos(\omega t + \overline{\theta}) \\ \frac{i(t)}{\overline{r}} \sin(\omega t + \overline{\theta}) \end{bmatrix} \\ &= \frac{\alpha}{C} \begin{bmatrix} \frac{\overline{r}}{2} - \frac{\beta\overline{r}^3}{8} \\ 0 \end{bmatrix} + \frac{\kappa\omega}{2\pi C} \int_0^{\frac{2\pi}{\omega}} \begin{bmatrix} -\frac{i(t)\overline{r}}{\overline{r}} \cos(\omega t + \overline{\theta}) \\ \frac{i(t)\overline{r}}{\overline{r}^2} \sin(\omega t + \overline{\theta}) \end{bmatrix} dt. \end{aligned} \tag{21}$$

Recalling the instantaneous and average active and reactive power definitions in (2) and (3), respectively, we obtain the averaged dynamics in (21) by (15) after dropping $\mathcal{O}(\varepsilon^2)$ terms; see [37] for the detailed calculations leveraging integration by parts and averaging arguments.

Under assumptions (A1), (A2), and (A3), by standard averaging arguments [13, Theor. 10.4], there exists an $\varepsilon_1^*$ sufficiently small so that for all $0 < \varepsilon < \varepsilon_1^*$, the solution of the averaged VOC dynamics (15) is $\mathcal{O}(\varepsilon)$ close to the solution of the original VOC dynamics (11) for times $t \in [0, t^*/\varepsilon]$. We proceed by comparing the averaged VOC system (15) with the droop control system (13).

*2) Correspondence of Phase Dynamics:* We first study the phase dynamics (15b). The VOC system (11) is assumed to evolve in quasistationary sinusoidal steady state with a small initial (at time $t = 0$) $\mathcal{O}(\varepsilon)$ difference from the harmonic droop signals. Recall that in the quasiharmonic limit, there exists an $\varepsilon_2^*$ sufficiently small so that for all $0 < \varepsilon < \varepsilon_2^*$, the solution of the VOC dynamics (11) is $\mathcal{O}(\varepsilon)$ close to the solution of a harmonic oscillator with radius $\overline{r}_{j,\mathrm{eq}}$ for $t \in [0, t^*]$; see [13] and [22].

[3]For notational simplicity, we drop the subscript $j$ from the variables $[r, \theta]^{\mathrm{T}}$, $[\overline{r}, \overline{\theta}]^{\mathrm{T}}$, $\kappa, i, u$, indexing the $j$th inverter in (19)–(21).

In particular, for $t \in [0, t^*]$, the solution $\overline{\theta}_j(t)$ of the averaged phase dynamics (15b) is $\mathcal{O}(\varepsilon)$ close to the solution of

$$\frac{d}{dt}\overline{\theta}_j = \frac{\kappa_j}{C\overline{r}_{j,\mathrm{eq}}^2}\overline{Q}_j$$

where we disregard the amplitude dynamics (15a), and replace $\overline{r}_j(t)$ in (15b) by $\overline{r}_{j,\mathrm{eq}}$ (whose closed form will be discussed).

For the following arguments, let $0 \leq \varepsilon \leq \min\{\varepsilon_1^*, \varepsilon_2^*\}$. Observe that the phase dynamics of a droop-controlled inverter (13) correspond with the ac-cycle-averaged dynamics of a VO-controlled inverter (11)—up to an order $\mathcal{O}(\varepsilon)$ mismatch—if we pick the reactive power setpoint $\overline{Q}_j^*$ and the frequency-droop coefficient $n_j$ as follows:

$$\overline{Q}_j^* = 0, \quad n_j = \frac{\kappa_j}{\overline{r}_{j,\mathrm{eq}}^2 C}. \tag{22}$$

*3) Correspondence of Amplitude Dynamics:* Next, we consider the amplitude dynamics (15a) and its equilibrium terminal voltage profile. For the network of VO-controlled inverters, the steady-state voltage profile is recovered from the solution of the following $N$ nonlinear equations:

$$0 = \frac{\alpha}{2C}\left(\overline{r}_{j,\mathrm{eq}} - \frac{\beta}{4}\overline{r}_{j,\mathrm{eq}}^3\right) - \frac{\kappa_j \overline{P}_{j,\mathrm{eq}}}{C\overline{r}_{j,\mathrm{eq}}}, \quad \forall\, j = 1, \ldots, N. \tag{23}$$

Rearranging terms in (23), we obtain the following power balance condition for the $j$th inverter:

$$\frac{\alpha\beta}{8}\overline{r}_{j,\mathrm{eq}}^4 - \frac{\alpha}{2}\overline{r}_{j,\mathrm{eq}}^2 + \kappa_j \overline{P}_{j,\mathrm{eq}} = 0. \tag{24}$$

The positive roots of the above equation are given by

$$\overline{r}_{j,\mathrm{eq}} = \left[\frac{2\alpha \pm 2\sqrt{\alpha^2 - 6k\kappa_j \overline{P}_{j,\mathrm{eq}}}}{3k}\right]^{\frac{1}{2}} \tag{25}$$

where we have used the fact that $\alpha\beta = 3k$ [see (8)]. Notice that these two roots are real-valued if and only if (16) holds. Around the high-voltage solution of (25) (denoted by $\overline{r}_{j,\mathrm{eq}}$ with a slight abuse of notation), the sensitivity of the active power injection with respect to a change in amplitude is

$$\kappa_j \frac{d\overline{P}_{j,\mathrm{eq}}}{d\overline{r}_{j,\mathrm{eq}}} = \alpha\left(\overline{r}_{j,\mathrm{eq}} - \frac{\beta}{2}\overline{r}_{j,\mathrm{eq}}^3\right), \quad \forall\, j = 1, \ldots, N. \tag{26}$$

In Theorem 3, we prove that this high-voltage solution is exponentially stable. Equation (26) can be placed in correspondence with the amplitude dynamics of a droop-controlled inverter (13). By an analogous reasoning as for the phase dynamics, there exists an $\varepsilon_3^*$ sufficiently small so that for all $0 < \varepsilon < \varepsilon_3^*$, the solution $\overline{r}_j(t)$ of the averaged amplitude dynamics (15a) satisfies—up to an $\mathcal{O}(\varepsilon)$ mismatch—the conditions of the stationary solution (26) (with fixed radius $\overline{r}_{j,\mathrm{eq}}$) for times $t \in [0, t^*]$.

For the following arguments, let $0 \leq \varepsilon \leq \min\{\varepsilon_1^*, \varepsilon_3^*\}$. Observe that the amplitude dynamics of a droop-controlled inverter (13) correspond with that of a VO-controlled inverter in (26)—up to an order $\mathcal{O}(\varepsilon)$ mismatch—if we pick the active power setpoint $\overline{P}_j^*$, terminal voltage setpoint $\overline{r}_j^*$, and the voltage-droop coefficient $m_j$ as follows:

$$\overline{P}_j^* = \overline{P}_{j,\mathrm{eq}},\ \overline{r}_j^* = \overline{r}_{j,\mathrm{eq}},\ m_j = -\kappa_j\left(\alpha\left(\overline{r}_{j,\mathrm{eq}} - \frac{\beta}{2}\overline{r}_{j,\mathrm{eq}}^3\right)\right)^{-1}.$$

Finally, to complete the proof, let $\varepsilon^* = \min\{\varepsilon_1^*, \varepsilon_2^*, \varepsilon_3^*\}$, and note that all arguments hold for the time scales $[0, t^*/\varepsilon^*] \cap [0, t^*]$ which equals $[0, t^*]$ for $\varepsilon^*$ sufficiently small. ■

## IV. Stability of VOC Amplitude and Phase Dynamics

In this section, we investigate the stability of the averaged VOC voltage dynamics (15). Our results are applicable to connected microgrid electrical networks with resistive interconnecting lines, and we place no restrictions on the network topology. Loads in the network are modeled as parallel connections of resistances and current sources/sinks (to simplify exposition, we refer to these as current sources subsequently).

### A. Microgrid Network Architecture

We assume balanced three-phase operation and all electrical quantities referred henceforth are with respect to a per-phase equivalent network. The microgrid electrical network is described by an undirected graph with inverters and/or loads in the system connected to the nodes of the graph, and edges represent interconnections through transmission lines. The nodes of the electrical network are collected in the set $\mathcal{A}$, and branches (edges) are collected in the set $\mathcal{E} := \{(j, \ell)\} \subset \mathcal{A} \times \mathcal{A}$. Let $\mathcal{N} := \{1, \ldots, N\} \subseteq \mathcal{A}$ denote nodes that the inverters are connected to; we will refer to this as the set of *boundary nodes*. Shunt loads—modeled as parallel combinations of resistances and/or constant (in a synchronous $dq$-frame) current sources—are connected to *interior nodes*. The set $\mathcal{I} := \mathcal{A} \setminus \mathcal{N}$ collects all of the interior nodes in the network.

Denote the vectors that collect the nodal current injections and node voltages in the network by $i_{\mathcal{A}}$ and $v_{\mathcal{A}}$, respectively. To be precise, $i_{\mathcal{A}}$ and $v_{\mathcal{A}}$ are real-valued functions of time. The coupling between the inverters is described by Kirchhoff's and Ohm's laws, which read in matrix-vector form as

$$i_{\mathcal{A}} = Q_{\mathcal{A}} v_{\mathcal{A}} \tag{27}$$

where entries of the *conductance matrix* $Q_{\mathcal{A}} \in \mathbb{R}^{|\mathcal{A}|\times|\mathcal{A}|}$ are

$$[Q_{\mathcal{A}}]_{j\ell} := \begin{cases} g_j + \sum_{(j,k)\in\mathcal{E}} g_{jk}, & \text{if } j = \ell \\ -g_{j\ell}, & \text{if } (j,\ell) \in \mathcal{E} \\ 0, & \text{otherwise} \end{cases} \tag{28}$$

with $g_j \in \mathbb{R}_{\geq 0}$ denoting the shunt (load) conductance at node $j$, and $g_{j\ell} = g_{\ell j} \in \mathbb{R}_{\geq 0}$ the conductance of the line $(j, \ell)$.

Let $i = [i_1, \ldots, i_N]^{\mathrm{T}}$ and $v = [v_1, \ldots, v_N]^{\mathrm{T}}$ be the vectors of inverter current injections and terminal voltages at the boundary nodes, and let $i_{\mathcal{I}}$ and $v_{\mathcal{I}}$ be the vectors collecting the current injections and nodal voltages for the interior nodes.[4] Entries of

[4]We drop the subscript $\mathcal{N}$ when referring to the current and voltage vectors corresponding to the boundary nodes.

$i_{\mathcal{I}}$ are nonzero only if the interior nodes are connected to current sources. With this notation, we can rewrite (27) as

$$\begin{bmatrix} i \\ i_{\mathcal{I}} \end{bmatrix} = \begin{bmatrix} Q_{\mathcal{N}\mathcal{N}} & Q_{\mathcal{N}\mathcal{I}} \\ Q_{\mathcal{N}\mathcal{I}}^{\mathrm{T}} & Q_{\mathcal{I}\mathcal{I}} \end{bmatrix} \begin{bmatrix} v \\ v_{\mathcal{I}} \end{bmatrix}. \tag{29}$$

Assuming that the submatrix $Q_{\mathcal{I}\mathcal{I}}$ is nonsingular,[5] the second set of equations in (29) can be uniquely solved for the interior voltages as $v_{\mathcal{I}} = Q_{\mathcal{I}\mathcal{I}}^{-1}(i_{\mathcal{I}} - Q_{\mathcal{N}\mathcal{I}}^{\mathrm{T}} v)$. Using this, we obtain

$$i = Qv + Q_{\mathcal{N}\mathcal{I}} Q_{\mathcal{I}\mathcal{I}}^{-1} i_{\mathcal{I}} \tag{30}$$

where the matrix $Q = (Q_{\mathcal{N}\mathcal{N}} - Q_{\mathcal{N}\mathcal{I}} Q_{\mathcal{I}\mathcal{I}}^{-1} Q_{\mathcal{N}\mathcal{I}}^{\mathrm{T}})$ is referred to as the *Kron-reduced conductance matrix*. This model reduction through a Schur complement of the conductance matrix is known as *Kron reduction* [21]. With a slight abuse of notation, we denote the effective shunt-conductance load for the $j$th inverter by $g_j$ (note that this is given by the $j$th non-negative row sum of the Kron-reduced conductance matrix $Q$), and the effective conductance of the $(j,\ell)$ line in the Kron-reduced electrical network by $g_{j\ell} = -[Q]_{j\ell}$ in all subsequent discussions. In addition, the shunt current source at the $j$th inverter recovered after Kron reduction, given by the $j$th entry of the vector $Q_{\mathcal{N}\mathcal{I}} Q_{\mathcal{I}\mathcal{I}}^{-1} i_{\mathcal{I}}$, will be denoted by $\iota_j \cos(\omega t + \gamma_j)$, where $\iota_j$ is the amplitude of the current source, and $\gamma_j$ is the phase offset with respect to the rotating reference frame established by $\omega$. With this notation, the average real and reactive power injections for the $j$th inverter are given by [16]

$$\begin{aligned} \overline{P}_j &= \frac{\overline{r}_j \iota_j}{2} \cos(\overline{\theta}_j - \gamma_j) + \frac{\overline{r}_j^2}{2} g_{jj} - \frac{\overline{r}_j}{2} \sum_{\ell=1, \ell \neq j}^{N} g_{j\ell} \overline{r}_\ell \cos(\overline{\theta}_{j\ell}) \\ \overline{Q}_j &= \frac{\overline{r}_j \iota_j}{2} \sin(\overline{\theta}_j - \gamma_j) - \frac{\overline{r}_j}{2} \sum_{\ell=1}^{N} g_{j\ell} \overline{r}_\ell \sin(\overline{\theta}_{j\ell}) \end{aligned} \tag{31}$$

where we use the shorthand $\overline{\theta}_{j\ell} := \overline{\theta}_j - \overline{\theta}_\ell$, and $(\overline{r}_j \iota_j/2) \cos(\overline{\theta}_j - \gamma_j)$ and $(\overline{r}_j \iota_j/2) \sin(\overline{\theta}_j - \gamma_j)$ are the active and reactive power drawn by the equivalent current source at the $j$th-inverter terminals (after Kron reduction). For these networks, we obtain the following well-posedness and convergence result.

*Theorem 2 (Convergence of VOC):* Consider the interconnected averaged VOC dynamics (15) with real and reactive power injections given by (31). Suppose that the terminal voltage amplitudes are upper bounded by the open-circuit voltage $\overline{r}^{\mathrm{oc}} := \sqrt{4\alpha/3k}$.[6] Assume further that the network and oscillator parameters satisfy $\forall j \in \mathcal{N}$

$$\frac{16}{81} (\alpha - \kappa_j g_{jj})^3 \geq k \kappa_j^2 \left( \iota_j + \overline{r}^{\mathrm{oc}} \sum_{\ell=1, \ell \neq j}^{N} g_{j\ell} \right)^2. \tag{32}$$

Then, for all initial conditions $(\overline{r}_0, \overline{\theta}_0) \in \mathbb{R}^N_{\geq 0} \times \mathbb{T}^N$ that satisfy

$$\overline{r}_j^{\mathrm{low}} := \sqrt{\frac{4}{9k}(\alpha - \kappa_j g_{jj})} \leq \overline{r}_{0,j} \leq \overline{r}^{\mathrm{oc}}, \ \forall j \in \mathcal{N} \tag{33}$$

the dynamics (15), (31) have positive radii $\overline{r}_j(t) \geq \overline{r}_j^{\mathrm{low}}$ for all $j \in \mathcal{N}$ and for all $t \geq 0$, and they ultimately converge to a set of equilibria as $t \to \infty$.

We briefly discuss the assumptions in Theorem 2. Condition (32) ensures that the radii $\overline{r}_j(t)$ remain greater than a strictly positive value $\overline{r}_j^{\mathrm{low}}$ given in (33). Condition (32) is always guaranteed for sufficiently small current and resistive loads and a weakly coupled network, and it can be satisfied by choosing the ratio of design parameters $\alpha/\kappa_j$ sufficiently large. The proof of Theorem 2 relies on a gradient formulation of the system dynamics and LaSalle arguments.

*Proof of Theorem 2:* Inspired by [38] and [39], we begin by rewriting the system (15), (31) in gradient form as

$$\dot{\overline{r}}_j =: p_j(\overline{r}, \overline{\theta}) = -\nabla_{\overline{r}_j} H(\overline{r}, \overline{\theta}) \tag{34a}$$

$$\dot{\overline{\theta}}_j =: q_j(\overline{r}, \overline{\theta}) = -\frac{1}{\overline{r}_j^2} \nabla_{\overline{\theta}_j} H(\overline{r}, \overline{\theta}) \tag{34b}$$

where $[\overline{r}, \overline{\theta}]^{\mathrm{T}} = [\overline{r}_1, \ldots, \overline{r}_N, \overline{\theta}_1, \ldots, \overline{\theta}_N]^{\mathrm{T}}$, and the potential $H : \mathbb{R}^N_{\geq 0} \times \mathbb{T}^N \to \mathbb{R}$ is defined as

$$\begin{aligned} H(\overline{r}, \overline{\theta}) := \sum_{j=1}^{N} \Bigg[ &\frac{\alpha}{4C} \left( -\overline{r}_j^2 + \frac{\beta}{8} \overline{r}_j^4 \right) + \frac{\kappa_j \iota_j}{2C} \overline{r}_j \cos(\overline{\theta}_j - \gamma_j) \\ &+ \frac{\kappa_j}{4C} g_{jj} \overline{r}_j^2 - \frac{\kappa_j}{2C} \sum_{\ell=1, \ell \neq j}^{N} \overline{r}_j \overline{r}_\ell g_{j\ell} \cos(\overline{\theta}_{j\ell}) \Bigg]. \end{aligned}$$

Notice that the phase dynamics (34b) are not defined for $\overline{r}_j = 0$, and the notion of a *radius* is ill-posed whenever $\overline{r}_j \leq 0$. Hence, we first establish conditions such that the radii remain greater than $\chi > 0$, that is, we seek conditions that ensure the set

$$\Omega_\chi := \left\{ (\overline{r}, \overline{\theta}) \in \mathbb{R}^N_{\geq 0} \times \mathbb{T}^N : \chi \leq \overline{r}_j \leq \overline{r}^{\mathrm{oc}}, \ \forall j \in \mathcal{N} \right\}$$

is positively invariant. To this end, we evaluate cases such that $p_j(\overline{r}, \overline{\theta}) \geq 0$ whenever $(\overline{r}, \overline{\theta}) \in \Xi_j \times \mathbb{T}^N$, where

$$\Xi_j := \left\{ \overline{r} \in \mathbb{R}^N_{\geq 0} : \overline{r}_j = \chi_j, \chi_\ell \leq \overline{r}_\ell \leq \overline{r}^{\mathrm{oc}}, \ell \neq j \right\} \tag{35}$$

with $\chi_j$ and $\chi_\ell$ yet to be determined. In particular, $\forall j \in \mathcal{N}$

$$\begin{aligned} &p_j(\overline{r}, \overline{\theta})|_{(\overline{r}, \overline{\theta}) \in \Xi_j \times \mathbb{T}^N} \\ &= \Bigg[ \frac{\alpha}{2C} \left( \overline{r}_j - \frac{\beta}{4} \overline{r}_j^3 \right) - \frac{\kappa_j \iota_j}{2C} \cos(\overline{\theta}_j - \gamma_j) \\ &\qquad - \frac{\kappa_j \overline{r}_j}{2C} g_{jj} + \frac{\kappa_j}{2C} \sum_{\ell=1, \ell \neq j}^{N} g_{j\ell} \overline{r}_\ell \cos(\overline{\theta}_{j\ell}) \Bigg] \Bigg|_{(\overline{r}, \overline{\theta}) \in \Xi_j \times \mathbb{T}^N} \\ &\geq \frac{\alpha}{2C} \left( \chi_j - \frac{\beta}{4} \chi_j^3 \right) - \frac{\kappa_j}{2C} \left( \iota_j + \chi_j g_{jj} + \overline{r}^{\mathrm{oc}} \sum_{\ell=1, \ell \neq j}^{N} g_{j\ell} \right) \geq 0 \end{aligned}$$

which holds if and only if there exists a $\chi_j \in \mathbb{R}_{>0}$ so that

$$h_j(\chi_j) := \frac{\alpha\beta}{4} \chi_j^3 - (\alpha - \kappa_j g_{jj}) \chi_j + \kappa_j \iota_j + \kappa_j \overline{r}^{\mathrm{oc}} \sum_{\ell=1, \ell \neq j}^{N} g_{j\ell}$$

is nonpositive. Since $h_j$ is a cubic polynomial with a leading-order positive coefficient $\alpha\beta/4$, the question *whether there is a* $\chi_j > 0$ *so that* $h_j(\chi_j) < 0$ can be answered by calculating the positive maximum/minimum $\chi_j^*$ (the root of the equation

[5] This holds true, in general, for RLC networks, except for some pathological cases, see [20]. For the resistive networks we consider in this work, $Q_{\mathcal{I}\mathcal{I}}$ is always nonsingular due to irreducible diagonal dominance [21].

[6] The open-circuit voltage of the VO-controlled inverter is defined as the voltage obtained when no current is drawn from it. It is recovered from the high-voltage solution of (25) by setting $\overline{P}_{j,\mathrm{eq}} = 0$.

$\partial h_j/\partial \chi_j = 0$) and verifying that $h_j(\chi_j^*) \leq 0$.[7] The positive root $\chi_j^*$ is denoted by $\overline{r}_j^{\rm low}$ in (33) and $h_j(\overline{r}_j^{\rm low}) \leq 0$ if and only if (32) holds true. Hence, under condition (32), we have positive invariance of the set

$$\Omega := \left\{(\overline{r},\overline{\theta}) \in \mathbb{R}^N_{\geq 0} \times \mathbb{T}^N : \overline{r}^{\rm low} \leq \overline{r}_j^{\rm low} \leq \overline{r}_j \leq \overline{r}^{\rm oc},\ \forall\, j \in \mathcal{N}\right\}$$

where $\overline{r}^{\rm low} := \min_{j\in\mathcal{N}} \overline{r}_j^{\rm low}$. Every trajectory originating in $\Omega$ remains in $\Omega$, that is, $\overline{r}_j(t)$ is greater than $\overline{r}_j^{\rm low}$, $\forall\, t \geq 0$.

The level sets of $H(\overline{r},\overline{\theta})$ are closed (due to continuity), bounded in $\overline{\theta}$ (due to boundedness of the trigonometric nonlinearities), and radially unbounded in $\overline{r}$. Moreover, $H(\overline{r},\overline{\theta})$ is nonincreasing along trajectories, since

$$\begin{aligned}\dot{H}(\overline{r},\overline{\theta}) &= -\sum_{j=1}^{N}\left(\nabla_{\overline{r}_j} H(\overline{r},\overline{\theta}))\right)^2 + \left(\frac{1}{\overline{r}_j}\nabla_{\overline{\theta}_j} H(\overline{r},\overline{\theta}))\right)^2 \\ &= -\sum_{j=1}^{N} p_j(\overline{r},\overline{\theta})^2 + \overline{r}_j^2 q_j(\overline{r},\overline{\theta})^2 \leq 0.\end{aligned}$$

Thus, the sublevel sets of $H(\overline{r},\overline{\theta})$ are compact and forward invariant, and we conclude by LaSalle's invariance principle [13, Theor. 4.4] that the dynamics (15), (31) converge to the largest positively invariant set contained in

$$\left\{(\overline{r},\overline{\theta}) \in \Omega : H(\overline{r},\overline{\theta}) \leq H(\overline{r}_0,\overline{\theta}_0), \dot{H}(\overline{r},\overline{\theta}) = 0\right\}$$

where we incorporated the positive invariance of $\Omega$. The condition $\dot{H}(\overline{r},\overline{\theta}) = 0$ identifies the set of equilibria and points of zero amplitude $\overline{r}_j = 0$. Since the latter set is excluded from $\Omega$, all trajectories originating in $\Omega$ converge to the nonempty set of equilibria. ■

Next, we linearize the system around an equilibrium point $(\overline{r}_{\rm eq},\overline{\theta}_{\rm eq})$. The Jacobian of the system around the equilibrium point can be partitioned into blocks as follows:

$$J = \left[\begin{array}{c|c} J_{\rm A} & J_{\rm B} \\ \hline J_{\rm C} & J_{\rm D}\end{array}\right]. \tag{36}$$

The entries of $J_{\rm A}$, $J_{\rm B}$, $J_{\rm C}$, and $J_{\rm D}$ are specified as

$$[J_{\rm A}]_{j\ell} = \begin{cases} \frac{\alpha}{2C}(1-\frac{3}{4}\overline{r}_{j,{\rm eq}}^2) - \frac{\kappa_j}{2C}g_{jj} & \text{if } j=\ell \\ \frac{\kappa_j}{2C}g_{jl}\cos(\overline{\theta}_{{\rm eq},j\ell}) & \text{if } j\neq\ell\end{cases}$$

$$[J_{\rm B}]_{j\ell} = \begin{cases} 0 & \text{if } j=\ell \\ -\frac{\kappa_j}{2C}g_{j\ell}\overline{r}_{j,{\rm eq}}\sin(\overline{\theta}_{{\rm eq},j\ell}) & \text{if } j\neq\ell\end{cases}$$

$$[J_{\rm C}]_{j\ell} = \begin{cases} 0 & \text{if } j=\ell \\ \frac{\kappa_j}{2C\overline{r}_{j,{\rm eq}}}g_{j\ell}\sin(\overline{\theta}_{{\rm eq},j\ell}) & \text{if } j\neq\ell\end{cases}$$

$$[J_{\rm D}]_{j\ell} = \begin{cases} \frac{\kappa_j}{2C\overline{r}_{j,{\rm eq}}}\left(\iota_j\cos(\overline{\theta}_{j,{\rm eq}}-\gamma_j) \right. \\ \left. -\sum_{\ell=1,\ell\neq j}^{N}\overline{r}_{\ell,{\rm eq}}\cos(\overline{\theta}_{j\ell,{\rm eq}})\right) & \text{if } j=\ell \\ -\frac{\kappa_j}{2C\overline{r}_{j,{\rm eq}}}g_{j\ell}\overline{r}_{\ell,{\rm eq}}\cos(\overline{\theta}_{{\rm eq},j\ell}) & \text{if } j\neq\ell\end{cases}$$

[7]For $h(x) = ax^3 - bx + c$, we obtain the extremal points by $0 = \partial h/\partial x = 3ax^2 - b$. If we assume that $a, b > 0$, then the positive root is $x^* = \sqrt{b/3a}$. We then obtain $h(x^*) = a(b/3a)\sqrt{b/3a} - b\sqrt{b/3a} + c$. Notice that $h(x^*) \leq 0$ if and only if $a(b/3a) - b \leq -c\sqrt{3a/b}$. This is equivalent to the condition $(4/27)b^3 \geq ac^2$.

where $\overline{\theta}_{{\rm eq},jl} := \overline{\theta}_{j,{\rm eq}} - \overline{\theta}_{l,{\rm eq}}$. It is evident that when the angle differences between the nodes are small, that is, $\sin(\overline{\theta}_{j,{\rm eq}} - \overline{\theta}_{\ell,{\rm eq}}) \approx 0$, the system becomes *decoupled*, that is, the Jacobian (36) becomes block diagonal. In spirit, similar observations are frequently leveraged in analyzing bulk power system dynamics in a variety of contexts [16]. Next, we scrutinize the amplitude and phase dynamics under this decoupling assumption. In particular, we assume the phase offsets (respectively, amplitudes) to be constant at their equilibrium values in the averaged amplitude (respectively, phase) dynamics in (15a) [respectively, (15b)]. We are then able to derive sufficient conditions for the exponential stability of amplitude and phase dynamics.

### B. Amplitude Dynamics in Decoupled Settings

Under the decoupling approximations described before, the phase offsets are fixed to their equilibrium values, that is, $\overline{\theta}_j = \overline{\theta}_{j,{\rm eq}}$, $\forall\, j \in \mathcal{N}$; following which the terminal voltage amplitude dynamics, recovered from (15a) and (31) are given by

$$\begin{aligned}\dot{\overline{r}}_j = \frac{\alpha}{2C}\left(\overline{r}_j - \frac{\beta}{4}\overline{r}_j^3\right) - \frac{\iota_j\kappa_j}{2C}\cos(\overline{\theta}_{j,{\rm eq}} - \gamma_j) \\ - \frac{\kappa_j}{2C}g_{jj}\overline{r}_j + \frac{\kappa_j}{2C}\sum_{\ell=1,\ell\neq j}^{N} g_{j\ell}\overline{r}_\ell\cos(\overline{\theta}_{j\ell,{\rm eq}}).\end{aligned} \tag{37}$$

*Theorem 3 (Local Exponential Stability of Decoupled Amplitude Dynamics):* Consider the decoupled terminal voltage amplitude dynamics in (37). Suppose that each inverter is loaded according to (16). If an equilibrium $\overline{r}_{j,{\rm eq}}$ satisfies

$$\overline{r}_j^{\rm low} < \overline{r}_{j,{\rm eq}} \leq \overline{r}^{\rm oc},\ \forall\, j \in \mathcal{N} \tag{38}$$

then it is locally exponentially stable.

*Proof of Theorem 3:* For small perturbations about the equilibrium point $\overline{r}_{\rm eq} = [\overline{r}_{1,{\rm eq}},\ldots,\overline{r}_{N,{\rm eq}}]^{\rm T}$ of (23), we express $\overline{r} = \overline{r}_{\rm eq} + \widetilde{r}$, where $\widetilde{r} := [\widetilde{r}_1,\ldots,\widetilde{r}_N]^{\rm T}$. Linearizing (37) around the equilibrium point (given by the solution of (23)), $\overline{r}_{\rm eq}$, we obtain $\dot{\widetilde{r}} = K\Gamma\widetilde{r}$, where $K := {\rm diag}\{\kappa_1,\ldots,\kappa_N\}$. The diagonal entries of $\Gamma$ are

$$[\Gamma]_{jj} = \frac{\alpha}{2C\kappa_j}\left(1 - \frac{3}{4}\beta\overline{r}_{j,{\rm eq}}^2\right) - \frac{1}{2C}\left(g_j + \sum_{\ell=1,\ell\neq j}^{N} g_{j\ell}\right).$$

Furthermore, the matrix $\Gamma$ is irreducible (due to connectivity) and symmetric since

$$[\Gamma]_{j\ell} = [\Gamma]_{\ell j} = \frac{1}{2C}g_{j\ell}\cos(\overline{\theta}_{j,{\rm eq}} - \overline{\theta}_{\ell,{\rm eq}}).$$

If we ensure

$$\frac{\alpha}{2\kappa_j}\left(1 - \frac{3}{4}\beta\overline{r}_{j,{\rm eq}}^2\right) - \frac{1}{2}g_j < 0 \tag{39}$$

then $\Gamma$ is negative definite (due to strictly irreducible diagonal dominance [40]). By Sylvester's inertia theorem [41], the inertia (i.e., the triple of positive, negative, and zero eigenvalues) of $\Gamma$ and $K\Gamma$ are identical since $\kappa_j > 0$, $\forall\, j \in \mathcal{N}$ and $K$ is positive definite. Consequently, $K\Gamma$ is negative definite, provided (39) is satisfied. The bounds in (38) are obtained by rearranging terms in (39). The upper bound in (38) is the open-circuit voltage. ■

### C. Phase Dynamics in Decoupled Settings

Under the decoupling assumptions, the terminal voltage amplitudes are fixed to their equilibrium values $\overline{r}_j = \overline{r}_{j,\mathrm{eq}},\ \forall\, j \in \mathcal{N}$ and the phase dynamics (15b) and (31) are given by

$$\dot{\overline{\theta}}_j = \frac{\kappa_j}{2C\overline{r}_{j,\mathrm{eq}}}\left(\iota_j \sin(\overline{\theta}_j - \gamma_j) - \sum_{\ell=1,\ell\neq j}^{N} g_{j\ell}\overline{r}_{\ell,\mathrm{eq}} \sin(\overline{\theta}_{j\ell})\right). \tag{40}$$

Analysis of the decoupled phase dynamics (40) with coupled oscillator theory [42], [43] leads to the following result.

*Theorem 4 (Local Exponential Stability of Decoupled Phase Dynamics):* Consider the decoupled phase dynamics (40). Assume that there exists an equilibrium $\overline{\theta}_{j,\mathrm{eq}}$ so that

$$|\overline{\theta}_{j\ell,\mathrm{eq}}| < \frac{\pi}{2} \quad \text{and} \quad |\overline{\theta}_{j,\mathrm{eq}} - \gamma_j| > \frac{\pi}{2},\ \forall j,\ell \in \mathcal{N}. \tag{41}$$

If there is at least one constant current load, then the equilibrium $\overline{\theta}_{j,\mathrm{eq}}$ is locally exponentially stable. Without constant current loads, the phase-synchronized equilibrium manifold $\overline{\theta}_{j,\mathrm{eq}} = \overline{\theta}_{\ell,\mathrm{eq}}$ for all $j,\ell \in \mathcal{N}$ is locally exponentially stable.

Condition (41) identifies the equilibria corresponding to small reactive power flows (as suggested by the condition $|\overline{\theta}_{j\ell,\mathrm{eq}}| < \pi/2$) and requires the local current sources to inject reactive power (as suggested by the condition $|\overline{\theta}_{j,\mathrm{eq}} - \gamma_j| > \pi/2$). Without current loads, the phase synchronization result perfectly matches our previous experimental results in [5] and [8].

*Proof of Theorem 4:* Linearization of (40) around the equilibrium point $\overline{\theta}_{\mathrm{eq}}$ yields $\dot{\widetilde{\theta}} = K\Theta M\widetilde{\theta}$, where $\overline{\theta} = \overline{\theta}_{\mathrm{eq}} + \widetilde{\theta}$, $K := \mathrm{diag}\{\kappa_1/\overline{r}_{1,\mathrm{eq}}, \ldots, \kappa_N/\overline{r}_{N,\mathrm{eq}}\}$, and $M := \mathrm{diag}\{\overline{r}_{1,\mathrm{eq}}, \ldots, \overline{r}_{N,\mathrm{eq}}\}$. The matrix $\Theta$ is irreducible (due to connectivity), and symmetric with offdiagonal entries

$$[\Theta]_{j\ell} = [\Theta]_{\ell j} = \frac{g_{j\ell}}{2C}\cos(\overline{\theta}_{j\ell,\mathrm{eq}}).$$

The diagonal entries of $\Theta$ are given by

$$[\Theta]_{jj} := \frac{\iota_j}{2C\overline{r}_{j,\mathrm{eq}}}\cos(\overline{\theta}_{j,\mathrm{eq}} - \gamma_j) - \sum_{\ell=1,\ell\neq j}^{N} [\Theta]_{j\ell}.$$

Under assumption (41), the offdiagonal entries $[\Theta]_{j\ell}$ are nonnegative, and all row sums are nonpositive. If there is at least one constant current load, the associated row sum is strictly negative. Hence, $\Theta$ is irreducibly diagonal dominant (due to connectivity) and, thus, also nonsingular [40, Cor. 6.2.27]. It follows that $\Theta$ is negative definite, and the equilibrium $\overline{\theta}_{\mathrm{eq}}$ is isolated and locally exponentially stable. In the absence of local current loads, the negative Jacobian $-\Theta$ is a Laplacian matrix associated with an undirected and connected graph. For this matrix, the phase-synchronized equilibrium manifold is locally exponentially stable. See [43, Theor. 5.1] for details.

The eigenvalues of the matrix $(K\Theta)M$ are the same as $M(K\Theta)$. Since $K, M$ are diagonal and $\Theta$ is symmetric, again by Sylvester's inertia theorem [41], the inertia (i.e., the triple of positive, negative, and zero eigenvalues) of $\Theta$ and $MK\Theta$ are identical since $\kappa_j > 0, \overline{r}_j > 0,\ \forall\, j \in \mathcal{N}$. Consequently, $K\Theta M$ is negative definite and, therefore, the phase dynamics are locally exponentially stable, provided that (41) is satisfied. ■

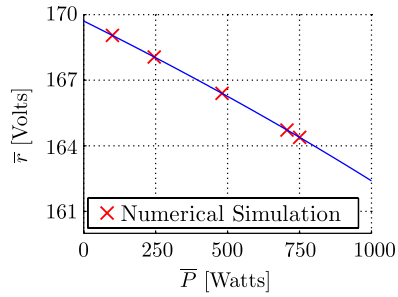


Fig. 3. Voltage-power characteristic (25) for an inverter superimposed to time-domain simulations of the nonaveraged nonlinear model (11) run out to steady state.

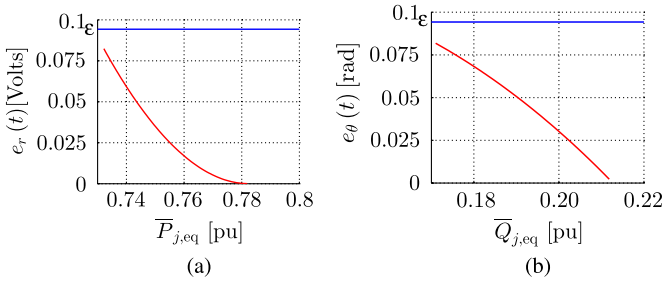


Fig. 4. Differences in: (a) equilibrium-voltages and (b) phase-offsets when comparing VOC and droop control.

## V. Reverse Engineering Droop Control, Convergence Rates, and Numerical Validation

Simulations in this section focus on corroborating the averaging analysis and the correspondence established with droop control. In addition, we discuss the load-sharing capabilities afforded by VOC. Finally, we comment on implications of the quasiharmonic limit $\varepsilon \searrow 0$ on the VOC convergence speed.

### A. Correspondence Between VOC and Droop Control

First, we validate the averaging analysis by focusing on the expression in (25). In particular, the voltage regulation curve for VOC [from (25)] is plotted in Fig. 3 and the analytical expression is validated by comparison with simulations of the original nonlinear and nonaveraged Van der Pol oscillator model (11) run out to steady state.

Next, we focus on the correspondences established between VOC and droop control. To this end, we model a single 15-kW three-phase inverter connected to a load which draws a constant current at a lagging power factor of 0.85. Suppose a Van der Pol oscillator-based controller (parameters are listed in the Appendix) supplies 0.78-p.u. active power and 0.21-p.u. reactive power in steady state. A corresponding droop controller is derived using the expressions in (17) and (18). Fig. 4(a) depicts $e_r(t)$ in steady state as the active power consumed by the load is varied. Fig. 4(b) depicts $e_\theta(t)$ recorded at time $t = 2.5$ s since the reactive power consumed by the load varies. Differences in both cases are of $\mathcal{O}(\varepsilon)$.

### B. Load Sharing and Economic Optimality

Consider the microgrid setting where $N$ inverters are connected in parallel across a balanced three-phase load. In this case, droop control (13) also achieves steady-state load sharing

or economic optimality. For resistive networks, it is known [2], [30] that the steady-state reactive power injection $\overline{Q}_{j,\mathrm{eq}}$ from the $j$th inverter is proportional to its rating $R_j$, that is

$$\frac{\overline{Q}_{j,\mathrm{eq}}}{R_j} = \frac{\overline{Q}_{\ell,\mathrm{eq}}}{R_\ell} \quad \forall\, j,\ell \in \{1,\dots,N\} \tag{42}$$

provided that the following holds:

$$\frac{\overline{Q}_j^*}{R_j} = \frac{\overline{Q}_\ell^*}{R_\ell}, \quad n_j R_j = n_\ell R_\ell \quad \forall\, j,\ell \in \{1,\dots,N\}.$$

Similarly, droop control can be designed to minimize an unconstrained economic dispatch of the reactive power injections

$$\min_{\{\overline{Q}_{j,\mathrm{eq}}\}_{j=1}^N} \quad \sum_{j=1}^N \lambda_j \overline{Q}_{j,\mathrm{eq}}^2 \tag{43}$$

with marginal costs $\lambda_i > 0$ provided that the reactive power setpoints and droop coefficients are selected as follows [14][8]:

$$\overline{Q}_j^* = 0, \quad \frac{n_j}{\lambda_j} = \frac{n_\ell}{\lambda_\ell}, \quad \forall\, j,\ell \in \{1,\dots,N\}. \tag{44}$$

The correspondences established in Theorem 1 allow us to translate these insights to the design of optimal current gains (i.e., the $\kappa$'s) in VO-controlled inverters (6) to achieve optimality in terms of reactive power production. In particular, leveraging (22) and based on (44), the following design achieves an optimal dispatch of reactive power generation:

$$\frac{\kappa_j}{\overline{r}_{j,\mathrm{eq}}^2 \lambda_j} = \frac{\kappa_\ell}{\overline{r}_{\ell,\mathrm{eq}}^2 \lambda_\ell}, \quad j,\ell \in \{1,\dots,N\}. \tag{45}$$

Similar load-sharing conditions have been obtained for inverters controlled as deadzone oscillators where all voltage waveforms perfectly synchronize (amplitude, frequency, and phase) [8]. In particular, picking the current gains $\kappa_j$ as

$$R_j \kappa_j = R_\ell \kappa_\ell, \quad \forall\, j,\ell \in \{1,\dots,N\} \tag{46}$$

ensures that the current injections are shared proportionally [8] and, thus, due to perfect synchronization of the voltage waveforms, the apparent power injections $\overline{S}_{j,\mathrm{eq}} = \overline{P}_{j,\mathrm{eq}} + \mathrm{j}\overline{Q}_{j,\mathrm{eq}}$ are shared proportionally in steady state

$$\frac{\overline{S}_{j,\mathrm{eq}}}{R_j} = \frac{\overline{S}_{\ell,\mathrm{eq}}}{R_\ell}, \quad \forall j,\ell \in \{1,\dots,N\}. \tag{47}$$

As a consequence, the average active and reactive injections are shared, and (42) is recovered as a special case. The results from Theorem 1 allow us to extend load-sharing results for VO-controlled inverters from a setting with perfectly synchronized waveforms to more general frequency-synchronized waveforms. Consider the closed-form high-voltage solution for the terminal voltage amplitude of the $j$th inverter in (25). When the oscillators are identical, the terminal voltage amplitudes synchronize if we pick the current gains as follows:

$$\kappa_j \overline{P}_{j,\mathrm{eq}} = \kappa_\ell \overline{P}_{\ell,\mathrm{eq}}, \quad \forall\, j,\ell \in \{1,\dots,N\}. \tag{48}$$

[8]Note that the two objectives (42) and (43) and the associated droop gains coincide for $R_j/\lambda_j = R_\ell/\lambda_\ell$ for all $j,\ell \in \{1,\dots,N\}$.

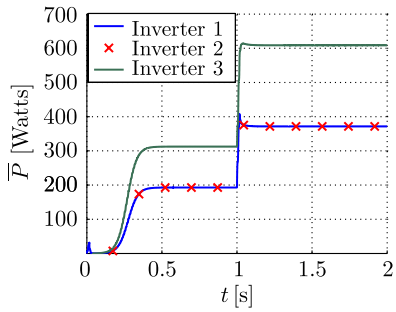


Fig. 5. Power sharing for three parallel VO-controlled inverters.

We simulate a case of power sharing between three identical VO-controlled inverters connected in a parallel configuration with current gains $\kappa = [2\ 2\ 1]^{\mathrm{T}}$. As shown in Fig. 5, two of the inverters share 25% of the load while the third inverter provides 50% of the load. A load step is applied at $t = 1$ s by doubling the active power demand. The inverters support the load in the ratio of their ratings even after the load step.

### C. Convergence Rate of a Van der Pol Oscillator

In this section, we discuss the implication of the quasiharmonic limit $\varepsilon \searrow 0$ on the time taken to converge to the limit cycle in an open-circuited Van der Pol oscillator, that is, when setting the driving term $u = 0$. From (10), we obtain

$$\frac{dr}{d\phi} = \frac{\varepsilon\alpha g\left(r\cos(\phi)\right)\cos(\phi)}{1 - \varepsilon\frac{\alpha}{r} g\left(r\cos(\phi)\right)\sin(\phi)}.$$

In the quasiharmonic limit $\varepsilon \ll 1$, we apply the series expansion $\varepsilon/(1-\varepsilon\cdot c) = \varepsilon + \mathcal{O}(\varepsilon^2)$ above to obtain

$$\frac{dr}{d\phi} = \varepsilon\left(\alpha g\left(r\cos(\phi)\right)\right)\cos(\phi) + \mathcal{O}(\varepsilon^2).$$

Averaging the above dynamics yields (up to $\mathcal{O}(\varepsilon^2)$ terms)

$$\frac{d\overline{r}}{d\overline{\phi}} = \frac{\alpha\varepsilon}{2}\left(\overline{r} - \frac{\beta}{4}\overline{r}^3\right). \tag{49}$$

Note that the locally stable equilibrium of the dynamics (49) is given by the open-circuit voltage $\overline{r}_{\mathrm{eq}} = \overline{r}^{\mathrm{oc}}$. We integrate both sides of (49), arbitrarily setting the limits from $0.1\overline{r}_{\mathrm{eq}}$ to $0.9\overline{r}_{\mathrm{eq}}$ (without loss of generality). The arc length traced during this transition $\phi_{\mathrm{s}}$ is given by the solution of

$$\left[-\frac{1}{4}\log\overline{r} + \frac{1}{8}\log\left|4 - \beta(\overline{r})^2\right|\right]_{0.1\overline{r}_{\mathrm{eq}}}^{0.9\overline{r}_{\mathrm{eq}}} = -\frac{1}{8}\varepsilon\phi_{\mathrm{s}}.$$

Evaluating the limits of this integral, we recover $\phi_{\mathrm{s}} \approx 6(\varepsilon\alpha)^{-1}$, which clearly indicates that the arc length $\phi_{\mathrm{s}}$ (proportional to a notion of convergence time to $\mathcal{O}(\varepsilon)$) traced before converging to the limit cycle is inversely proportional to $\varepsilon$. Fig. 6 plots $\phi_{\mathrm{s}}$ as a function of $\varepsilon$. The results from simulations of the original unforced nonlinear dynamics (10) (with $u = 0$) are superimposed to demonstrate the validity of the aforementioned analysis. We would like to remark that there is a fundamental tradeoff between harmonic content and dynamic response for the control strategy. In particular, to speed up dynamic response, we need a high value of $\varepsilon$; however, the amplitudes

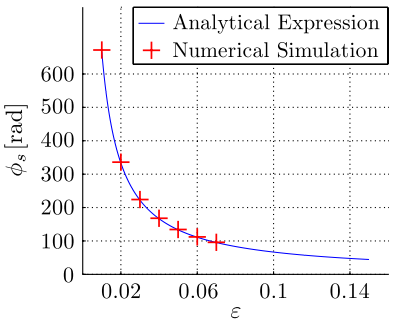


Fig. 6. Convergence rate of a Van der Pol oscillator.

of higher-order harmonics are directly proportional to $\varepsilon$. Our ongoing investigations attempt to uncover optimal oscillator parameters that achieve a desired tradeoff between higher-order harmonics and dynamic response.

## VI. Concluding Remarks

For a system of power-electronic inverters controlled as Van der Pol oscillators, we characterized the voltage dynamics in polar coordinates to establish two key results: 1) we derived a set of parameters for which the dynamics of the Van der Pol oscillators match the classical droop laws close to sinusoidal steady state, and 2) we established convergence of the Van der Pol oscillator dynamics to a set of potentially desirable equilibria. With this analysis, we are able to reverse engineer VOC, and ensure that it is backwards compatible with strategies developed for droop control. For instance, the choice of droop coefficients for network-wide economic optimality can be leveraged to inform VOC design.

While this paper takes a first step in comparing VOC and droop control, as part of future work, we will further compare the time-domain behavior of droop control and VOC in a variety of settings (e.g., three-phase systems, nonlinear loads, load steps, etc.). Extending the convergence and stability analysis to inductive networks while incorporating other load models and leveraging the averaged dynamics to design control strategies for general microgrid networks remains the focus of ongoing investigations. Yet another direction for future work is the application of singular perturbation methods and the method of multiple time scales to examine higher order harmonic content in VO-controlled inverter dynamics.

## Appendix

### A. Simulation Parameters

*Oscillator parameters:* $R = 10\ \Omega$, $L = 250\ \mu$H, $C = 28.14$ mF, $\sigma = 1$ S, $k = 4.1667 \times 10^{-5}$.

*Network Parameters (Power Sharing Simulation):* Before the load step: $g_{11} = 37.71$ S, $g_{22} = 27.87$ S, $g_{33} = 50.82$ S, $g_{12} = g_{21} = 8.2$ S, $g_{13} = g_{31} = 24.6$ S, $g_{23} = g_{32} = 16.4$ S. After the load step: $g_{11} = 37.07$ S, $g_{22} = 27.59$ S, $g_{33} = 48.28$ S, $g_{12} = g_{21} = 8.62$ S, $g_{13} = g_{31} = 25.86$ S, $g_{23} = g_{32} = 17.24$ S. Parameters correspond to the Kron-reduced network when the load is stepped from 20 to 10 $\Omega$.

## Acknowledgment

F. Dörfler would like to thank Rodolphe Sepulchre and Pierre Sacré; and B. Johnson would like to thank N. Ainsworth for insightful discussions.

## References

[1] M. C. Chandorkar, D. M. Divan, and R. Adapa, "Control of parallel connected inverters in standalone AC supply systems," *IEEE Trans. Ind. Appl.*, vol. 29, no. 1, pp. 136–143, Jan. 1993.
[2] Q.-C. Zhong, "Robust droop controller for accurate proportional load sharing among inverters operated in parallel," *IEEE Trans. Ind. Electron.*, vol. 60, no. 4, pp. 1281–1290, Apr. 2013.
[3] N. Pogaku, M. Prodanovic, and T. Green, "Modeling, analysis and testing of autonomous operation of an inverter-based microgrid," *IEEE Trans. Power Electron.*, vol. 22, no. 2, pp. 613–625, Mar. 2007.
[4] A. Bidram and A. Davoudi, "Hierarchical structure of microgrids control system," *IEEE Trans. Smart Grid*, vol. 3, no. 4, pp. 1963–1976, Dec. 2012.
[5] B. B. Johnson, S. V. Dhople, A. O. Hamadeh, and P. T. Krein, "Synchronization of nonlinear oscillators in an LTI electrical power network," *IEEE Trans. Circuits Syst. I, Reg. Papers*, vol. 61, no. 3, pp. 834–844, Mar. 2014.
[6] B. B. Johnson, S. V. Dhople, J. L. Cale, A. O. Hamadeh, and P. T. Krein, "Oscillator-based inverter control for islanded three-phase microgrids," *IEEE J. Photovolt.*, vol. 4, no. 1, pp. 387–395, Jan. 2014.
[7] S. V. Dhople, B. B. Johnson, and A. O. Hamadeh, "Virtual oscillator control for voltage source inverters," in *Proc. Allerton Conf. Commun., Control, Comput.*, 2013, pp. 1359–1363.
[8] B. B. Johnson, S. V. Dhople, A. O. Hamadeh, and P. T. Krein, "Synchronization of parallel single-phase inverters with virtual oscillator control," *IEEE Trans. Power Electron.*, vol. 29, no. 11, pp. 6124–6138, Nov. 2014.
[9] L. A. B. Tôrres, J. P. Hespanha, and J. Moehlis, "Synchronization of oscillators coupled through a network with dynamics: A constructive approach with applications to the parallel operation of voltage power supplies," *IEEE Trans. Autom. Control*, vol. 60, no. 12, pp. 3226–3241, Dec. 2015.
[10] L. A. B. Tôrres, J. P. Hespanha, and J. Moehlis, "Power supplies dynamical synchronization without communication," in *Proc. Power Energy Soc. Gen. Meeting*, 2012, pp. 1–6.
[11] R. Rand and P. Holmes, "Bifurcation of periodic motions in two weakly coupled Van der Pol oscillators," *Int. J. Non-Linear Mechan.*, vol. 15, no. 4, pp. 387–399, 1980.
[12] S. H. Strogatz, *Nonlinear Dynamics and Chaos: With Applications to Physics, Biology, Chemistry, Engineering*, 1st ed. Boulder, CO, USA: Westview, Jan. 2001.
[13] H. K. Khalil, *Nonlinear Systems*, 3rd ed. Upper Saddle River, NJ, USA: Prentice-Hall, 2002.
[14] F. Dörfler, J. W. Simpson-Porco, and F. Bullo, Breaking the hierarchy: distributed control & economic optimality in microgrids, 2014. [Online]. Available: http://arxiv.org/pdf/1401.1767v1.pdf
[15] M. Sinha, B. B. Johnson, N. G. Ainsworth, F. Dörfler, and S. V. Dhople, "Nonlinear supersets to droop control," presented at the IEEE Workshop Control and Modeling for Power Electronics, Vancouver, BC, Canada, 2015.
[16] P. Kundur, N. J. Balu, and M. G. Lauby, *Power System Stability and Control*. New York, NY, USA: McGraw-Hill, 1994, vol. 7.
[17] J. M. Guerrero, M. Chandorkar, T. Lee, and P. C. Loh, "Advanced control architectures for intelligent microgrids—Part I: Decentralized and hierarchical control," *IEEE Trans. Ind. Electron.*, vol. 60, no. 4, pp. 1254–1262, Apr. 2013.
[18] J. M. Guerrero, J. C. Vasquez, J. Matas, L. G. de Vicuña, and M. Castilla, "Hierarchical control of droop-controlled AC and DC microgrids—A general approach toward standardization," *IEEE Trans. Ind. Electron.*, vol. 58, no. 1, pp. 158–172, Jan. 2011.
[19] R. Majumder, A. Ghosh, G. Ledwich, and F. Zare, "Angle droop versus frequency droop in a voltage source converter based autonomous microgrid," in *Proc. IEEE Power Energy Soc. Gen. Meeting*, Jul. 2009, pp. 1–8.
[20] S. V. Dhople, B. B. Johnson, F. Dörfler, and A. O. Hamadeh, "Synchronization of nonlinear circuits in dynamic electrical networks with general topologies," *IEEE Trans. Circuits Syst. I, Reg. Papers*, vol. 61, no. 9, pp. 2677–2690, Sep. 2014.

[21] F. Dörfler and F. Bullo, "Kron reduction of graphs with applications to electrical networks," *IEEE Trans. Circuits Syst. I, Reg. Papers*, vol. 60, no. 1, pp. 150–163, Jan. 2013.
[22] A. Mauroy, P. Sacré, and R. J. Sepulchre, "Kick synchronization versus diffusive synchronization," in *Proc. IEEE Conf. Dec. Control*, 2012, pp. 7171–7183.
[23] S. E. Tuna, "Synchronization analysis of coupled lienard-type oscillators by averaging," *Automatica*, vol. 48, no. 8, pp. 1885–1891, 2012.
[24] P. T. Krein, J. Bentsman, R. M. Bass, and B. C. Lesieutre, "On the use of averaging for the analysis of power electronic systems," in *Proc. IEEE Power Electron. Specialists Conf.*, Jun. 1989, pp. 463–467.
[25] S. R. Sanders, J. M. Noworolski, X. Z. Liu, and G. C. Verghese, "Generalized averaging method for power conversion circuits," *IEEE Trans. Power Electron.*, vol. 6, no. 2, pp. 251–259, Apr. 1991.
[26] J. W. Kimball and P. T. Krein, "Singular perturbation theory for dc-dc converters and application to pfc converters," *IEEE Trans. Power Electron.*, vol. 23, no. 6, pp. 2970–2981, Nov. 2008.
[27] B. Lehman and R. M. Bass, "Switching frequency dependent averaged models for pwm dc-dc converters," *IEEE Trans. Power Electron.*, vol. 11, no. 1, pp. 89–98, Jan. 1996.
[28] V. A. Caliskan, O. Verghese, and A. M. Stankovic, "Multifrequency averaging of dc/dc converters," *IEEE Trans. Power Electron.*, vol. 14, no. 1, pp. 124–133, Jan. 1999.
[29] M. Sinha, F. Dörfler, B. B. Johnson, and S. V. Dhople, "Virtual oscillator control subsumes droop control," in *Proc. Amer. Control Conf.*, 2015, pp. 2353–2358.
[30] J. W. Simpson-Porco, F. Dörfler, and F. Bullo, "Synchronization and power sharing for droop-controlled inverters in islanded microgrids," *Automatica*, vol. 49, no. 9, pp. 2603–2611, 2013.
[31] J. W. Simpson-Porco, F. Dörfler, and F. Bullo, "Voltage stabilization in microgrids via quadratic droop control," in *Proc. IEEE Conf. Dec. Control*, 2013, pp. 7582–7589.
[32] J. Schiffer, D. Goldin, J. Raisch, and T. Sezi, "Synchronization of droop-controlled microgrids with distributed rotational and electronic generation," in *Proc. IEEE Conf. Dec. Control*, 2013, pp. 2334–2339.
[33] F. Wang, J. Duarte, and M. Hendrix, "Active and reactive power control schemes for distributed generation systems under voltage dips," in *Proc. IEEE Energy Convers. Congr. Expo.*, Sep. 2009, pp. 3564–3571.
[34] F. Z. Peng and J.-S. Lai, "Generalized instantaneous reactive power theory for three-phase power systems," *IEEE Trans. Instrum. Meas.*, vol. 45, no. 1, pp. 293–297, Feb. 1996.
[35] A. Yazdani and R. Iravani, *Voltage-Sourced Converters in Power Systems*. Hoboken, NJ, USA: Wiley, 2010.
[36] Q.-C. Zhong and Y. Zeng, "Parallel operation of inverters with different types of output impedance," in *Proc. Annu. Conf. IEEE Ind. Electron. Soc.*, Nov. 2013, pp. 1398–1403.
[37] M. Sinha, F. Dörfler, B. B. Johnson, and S. V. Dhople, Uncovering droop control laws embedded within the nonlinear dynamics of Van der Pol oscillators, 2014. [Online]. Available: http://arxiv.org/abs/1411.6973
[38] J. Schiffer, R. Ortega, A. Astolfi, J. Raisch, and T. Sezi, "Conditions for stability of droop-controlled inverter-based microgrids," *Automatica*, vol. 50, no. 10, pp. 2457–2469, Oct. 2014.
[39] R. Ortega, A. Van Der Schaft, B. Maschke, and G. Escobar, "Interconnection and damping assignment passivity-based control of port-controlled hamiltonian systems," *Automatica*, vol. 38, no. 4, pp. 585–596, 2002.
[40] R. Horn, and C. Johnson, *Matrix Analysis*. Cambridge, U.K.: Cambridge Univ. Press, 2012.
[41] D. Carlson and H. Schneider, "Inertia theorems for matrices: The semidefinite case," *J. Math. Anal. Appl.*, vol. 6, pp. 430–446, 1963.
[42] F. Dörfler, M. Chertkov, and F. Bullo, "Synchronization in complex oscillator networks and smart grids," *Proc. Nat. Acad. Sci.*, vol. 110, pp. 2005–2010, Feb. 2013.
[43] F. Dörfler and F. Bullo, "Synchronization in complex oscillator networks: A survey," *Automatica*, vol. 50, no. 6, pp. 1539–1564, 2014.

**Mohit Sinha** (S'15) received the B.Sc. degree in electrical engineering from the Indian Institute of Technology, Delhi, India, in 2011 and is currently pursuing the Ph.D. degree in electrical engineering from the University of Minnesota, Minneapolis, MN, USA.

His research interests include nonlinear system analysis and networked dynamical systems.

Dr. Sinha received an Electrical Engineering Department Fellowship in 2013.

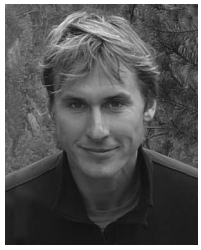

**Florian Dörfler** (M'15) received the Ph.D. degree in mechanical engineering from the University of California at Santa Barbara, Santa Barbara, CA, USA, in 2013, and a Diploma degree in engineering cybernetics from the University of Stuttgart, Stuttgart, Germany, in 2008.

From 2013 to 2014, he was an Assistant Professor at the University of California, Los Angeles, CA, USA. Currently, he is an Assistant Professor at the Automatic Control Laboratory at ETH Zürich, Zürich, Switzerland. His primary research interests are centered around distributed control, complex networks, and cyberphysical systems currently with applications in energy systems and smart grids.

Prof. Dörfler is a recipient of the 2009 Regents Special International Fellowship, the 2011 Peter J. Frenkel Foundation Fellowship, the 2010 ACC Student Best Paper Award, the 2011 O. Hugo Schuck Best Paper Award, the 2012–2014 Automatica Best Paper Award, and the 2015 UCSB ME Best PhD thesis award. As a co-advisor and a co-author, he has been a finalist for the ECC 2013 Best Student Paper Award.

**Brian B. Johnson** (S'08–M'13) received the B.S. degree in physics from Texas State University, San Marcos, TX, USA, in 2008 and the M.S. and Ph.D. degrees in electrical and computer engineering from the University of Illinois at Urbana-Champaign, Urbana, IL, USA, in 2010 and 2013, respectively.

Currently, he is an Electrical Engineer with the National Renewable Energy Laboratory, Golden, CO, USA. His research interests are in renewable energy systems, power electronics, and control systems.

Dr. Johnson was awarded a National Science Foundation Graduate Research Fellowship in 2010.

**Sairaj V. Dhople** (S'09–M'13) received the B.S., M.S., and Ph.D. degrees in electrical engineering from the University of Illinois, Urbana-Champaign, IL, USA, in 2007, 2009, and 2012, respectively.

Currently, he is an Assistant Professor in the Department of Electrical and Computer Engineering at the University of Minnesota, Minneapolis, MN, USA, where he is affiliated with the Power and Energy Systems Research Group. His research interests include modeling, analysis, and control of power electronics and power systems with a focus on renewable integration.

Dr. Dhople received the National Science Foundation CAREER Award in 2015 and currently serves as an Associate Editor for the IEEE TRANSACTIONS ON ENERGY CONVERSION.